Light deflection and birefringence in $(NH_4)_2SbF_5$ ferroelastic crystals

2000 J. Phys.: Condens. Matter 12 653

(http://iopscience.iop.org/0953-8984/12/5/313)

J. Phys.: Condens. Matter **12** (2000) 653–667. Printed in the UK PII: S0953-8984(00)08250-3

Light deflection and birefringence in $(NH_4)_2SbF_5$ ferroelastic crystals

Jean Bornarel†, Piotr Staniorowski‡ and Zbigniew Czapla‡

† Université Joseph Fourier, Laboratoire de Spectrométrie Physique (UMR 5588), BP no 87 - 38402 Saint-Martin-d'Hères Cedex, France

‡ Institute of Experimental Physics, University of Wroclaw, PI. M. Borna 9, PI-50-204 Wroclaw, Poland

Received 29 September 1999

Abstract. The light deflection phenomenon is studied in ammonium pentafluoro antimonate (APFA) crystals versus the laser beam incidence related to the twinned sample. The variations of the orientation of the deflected beams, as well as of their polarization are measured and theoretically explained. A simplified model allows one to establish analytical relations between the deflected beam angles (α and β) and the measured optical properties of the crystal. With a normal light beam incident on the sample, a linear dependence between $\sin^2\alpha$ and the birefringence is theoretically and experimentally demonstrated, which is interesting for further research and applications.

1. Introduction

The light phenomenon called deflection occurs when a laser beam crosses a polydomain ferroelastic or ferroelectric–ferroelastic crystal due to the orientation difference of optical indicatrices in the adjacent domains. The light deflection was first observed in Rochelle salt (Tsukamoto *et al* 1982), then in $Gd_2(MoO_4)_3$ and $Bi_4Ti_3O_{12}$ (Tsukamoto *et al* 1984), $RbHeSeO_4$ (Tsukamoto *et al* 1983, Tsukamoto 1984, Salvestrini *et al* 1997, Guilbert *et al* 1998), $KH_3(SeO_3)_2$ and $NaH_3(SeO_3)_2$ (Tsukamoto *et al* 1985), lithium ammonium tartrate monohydrate (LAT) (Koralewski and Szafranski 1989, Szafranski 1992) and sodium ammonium tartrate tetrahydrate (NAT) (Szafranski 1992, Koralewski and Szafranski 1988). A remarkable study was been accomplished by Meeks and Auld (1988) with the purpose to develop optical and acoustical devices with neodymium pentaphosphate crystals. A review was published in 1993 (Tsukamoto and Futuma 1993). More recently light deflection has been used to detect a phase transition existence in $KD_3(SeO_3)$, but the phenomenon can be mingled with the classical Frauenhofer diffraction by the domain texture (Hill and Ichiki 1964, Hill *et al* 1965). Light deflection has also been used to derive the orientation of a phase boundary in KHCO (Kinoshita *et al* 1994, Legrand *et al* 1998) and also in chiral smectic liquid crystals (Hatano *et al* 1993, Vehara *et al* 1996). The light deflection phenomenon is described in figure 1 in the simplest case, where only a permissible wall orientation appears in the crystal. The largest face of this plate-shaped sample is perpendicular to the domain walls. A nonpolarized laser beam hits the plane perpendicular to the domain walls and to the largest sample face. After crossing the multi-layered sample, six transmitted beams can be observed, as in figure 1(*b*). The direct (undeflected) beam D and the reflected beam R are non-polarized. The other beams are linearly polarized with the same polarizing plane of A

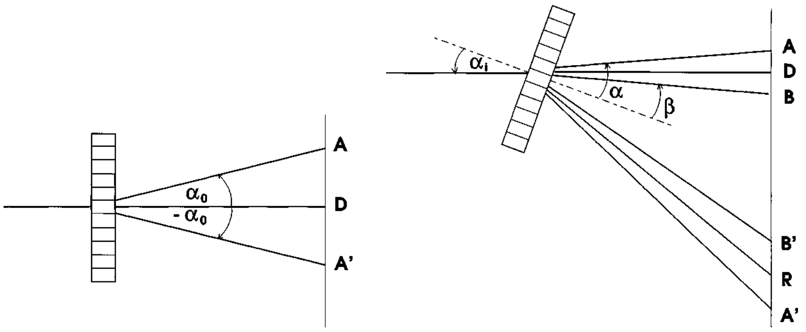

(*a*) (*b*)

Figure 1. Schematic illustration of the light deflection by a textured ferroelastic crystal. (*a*) The incidence angle α_i equals zero. Except for the transmitted beam, two deflected beams are observed with α_0 value for the deflection angle. (*b*) The incidence angle α_i is greater than $\alpha_{cri} = \alpha_0$ and six transmitted beams are observed.

and A′ perpendicular to the polarizing plane of B and B′. If the incidence angle α_i is smaller than a critical value α_{cri}, only the D, R, A and A′ beams are observed and this is obviously the case when α_i equals zero as shown in figure 1(*a*). Then the angle between the A and A′ beams and the normal to the largest sample face equals a characteristic value α_0. The intensity of the deflected beams changes with the number of the domain walls and with the optical properties of the crystal. The variation of the deflected beam intensities with the number of walls has been qualitatively demonstrated (Tsukamoto *et al* 1984) and the modification due to the indicatrices' orientation has been clarified only in the Rochelle salt (Tsukamoto *et al* 1982). The polarizing directions of the deflected beams were studied in $RbHSeO_4$ crystals especially (Tsukamoto *et al* 1984). Finally, the variation of the deflected beam orientations versus the incidence angle of the laser beam has often been studied. However, the total range 0–90° for the different angles is seldom explored. Furthermore, some discrepancies seem to exist between the experimental results and the numerical calculations, especially in $Gd_2(MoO_4)_3$ (GMO).

The purpose of the present paper, numbered I, is to firstly measure the deflection angles for α_i variation between 0° and 90° with a good accuracy for samples with different optical indicatrice orientations related to the domain walls; the crystal selected is $(NH_4)_2SbF_5$ (APFA). Secondly an analytical model is proposed to describe the variation of the deflected beams orientation versus the incidence angle and the optical properties of the crystal. A simplified model allows one to understand the relative importance of the birefringence and of the tilt angle between neutral lines of the optical indicatrices and the domain walls. This model could be useful for fundamental studies and applications as discussed in the last section. The following paper (Staniorowski and Bornarel 2000) demonstrates, with the help of results obtained in GMO crystals, the better accuracy of the method compared to that using the Huygens construction.

2. Experimental details

2.1. Crystal and samples

The APFA single crystals were grown by slow evaporation of aqueous solutions of stoichiometric quantities of NH_4F and SbF_3 with a small excess of H at 300 K. The crystal symmetry is orthorhombic (space group *Cmcm*) (Udovenko *et al* 1987, Waskowska and Czapla

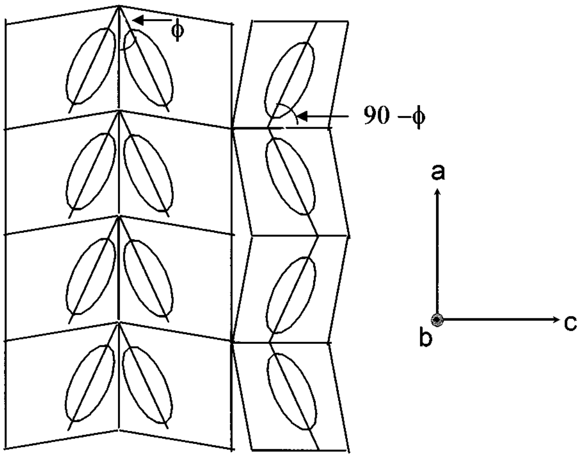

Figure 2. Positions of the optical indicatrices section in adjacent domains. The two permissible walls are observable in this (001) section.

1989, Czapla and Dacko 1994). Good quality crystals with a volume of 0.2–0.3 cm^3 were obtained during the four weeks of growth. This quality is checked by optical observations and dielectric property measurements (Bornarel *et al* 1997). The samples are obtained by cleavage in the (010) plane, then cut with a parallellepipedic shape in orthorhombic planes with a wire saw and polished with a wet silk cloth. The thickness of the samples in the b-direction is 1 mm. Previous experiments performed with similar samples allowed us to clarify the transitions where NH_4^+ ions play a great role, as demonstrated by nuclear magnetic resonance (NMR) and neutron scattering studies especially (Avkhutskii *et al* 1983, Nakamura 1986, Mukhopadhyay *et al* 1991, 1993). The existence of two phase transitions is demonstrated at temperatures 293 K and 169 K. The second order of the 293 K transition is established; the continuous character of the 169 K transition remains a more open question. APFA crystals exhibit a ferroelastic transition at 293 K between an orthorhombic phase and a monoclinic low-temperature phase (space group $C2/c$) (Udovenko *et al* 1987). Two permissible walls are possible in the (100) and (010) planes of the orthorhombic phase. In a (010) section, the angle 2ϕ between the axes of the optical indicatrices in two neighbouring domains equals 6° in a temperature range of 170–293 K for the first domain family illustrated in figure 2. In the second domain family this angle is 174°, i.e. $180 - 2\phi°$. The domain texture changes with the temperature: the domain wall density decreases with the temperature and only one orientation of the domain walls is usually observed below 200 K (Bornarel *et al* 1997).

2.2. Experiment set-up

Two different optical arrangements were used. Near room temperature the experiments are performed with the help of a goniometer, which was built in the laboratory. It is possible, using a He–Ne, 632 nm laser as a light source, to rotate the sample with regard to the incident laser beam step-by-step with an accuracy of 0.05°. The angle of deflection is determined by the aid of an automatically-rotated photodiode with the same accuracy. However, the repartition of the intensity of the deflected beams allows an accuracy on the deflected angles α and β equal to 0.2° at room temperature.

The optical measurements versus temperature are performed using a cryostat with a helium–gas exchange chamber, which allows optical observation and measurement along three perpendicular axes. The thermal gradient in the helium–gas chamber was controlled with the help of two platinum resistors placed just above and below the sample; the smallest thermal gradient can be 5 mK mm^{-1}. The temperature T reported is that of the low platinum resistor, which was measured with a precision of 2×10^{-3} K. All of the given results against temperature correspond to heating cycles with a temperature rate lower than 10^{-2} K min^{-1}. These conditions allow us to obtain reproducible results (Bornarel *et al* 1997). The optical measurements of the angle ϕ and the polarization orientation are performed with an accuracy of 0.2° and the Sénarmont method allows an accuracy equal 2×10^{-6} for the birefringence measurements.

3. Results

Several APFA samples (b plates) with similar shape and thickness were studied at 290 K. They exhibit domain textures with mean domain width of a few micrometres (Bornarel *et al* 1997). Figure 3 shows the results corresponding to a sample region with domain walls in the (001) planes called APFA1 walls. The dependence of the angles α and β, the deflection angles corresponding to the A and B rays, respectively, is given against the incidence angle α_i. The $\alpha(\alpha_i)$ and $\beta(\alpha_i)$ curves are well separated and the critical value α_{cri} equal 9.1° as the α_0 value. The orientation of the polarization of the A rays is perpendicular to that of the B rays. Both remain unchanged when α_i changes between 0–90°.

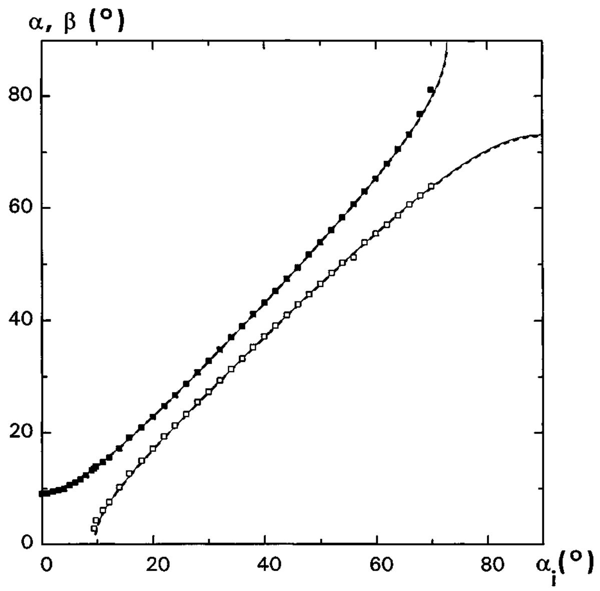

Figure 3. Variation of the α and β deflected angles against α_i for the APFA1 domain walls. The experimental results for the α (■) and β (□) angles, calculated values by the general model (full curve) and by the approximated case (broken curve) are shown.

Figure 4 shows the results corresponding to domain walls in (100) planes, called the APFA2 walls. The values of α_{cri} and α_0 appear to be similar to those obtained for APFA1 walls, but the curves $\alpha(\alpha_i)$ and $\beta(\beta_i)$ seem to cross each other in figure 4(*a*). The polarization of the A and B rays is always measured during the experiment and is given in figure 4(*b*). The polarization of these two rays is always perpendicular and in practice an exchange appears

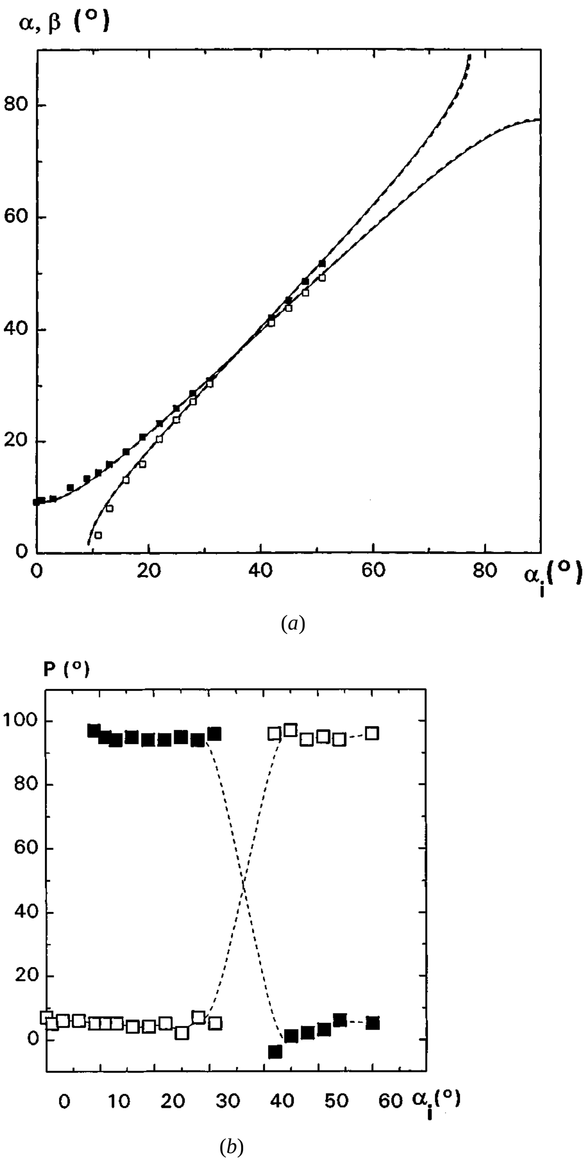

Figure 4. Variation of the (*a*) α and β deflected angles and (*b*) deflected rays'-polarization against α_i for the APFA2 domain walls. The definitions of the symbols and curves are given in figure 3.

around α_i equal to 35°, even if it is difficult to follow them in the 30–40° range because of the weak intensity of the deflected beams (a few per cent of the incident intensity).

The optical measurements performed during a heating cycle are summarized in figure 5. The variation of the tilt angle ϕ against the temperature T illustrates clearly the two phase transitions at the temperatures 293 K and 169 K (see figure 5(*a*)). Figure 5(*b*) gives the variation of the A rays α_0 angle against T and the intensity I_A of this beam is given, in arbitrary units.

In figure 5(*c*), the variation of the birefringence for a light propagating along the *b*-axis $\delta(\Delta n_b)$ is drawn against T during a heating cycle and a cooling cycle. These results are very

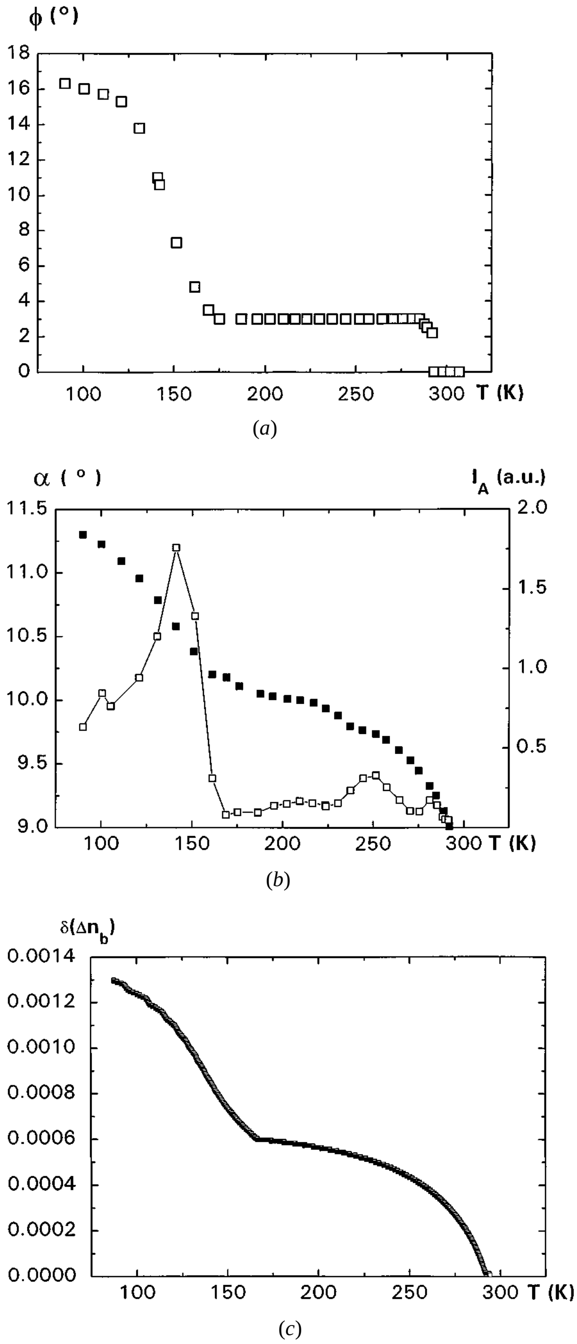

Figure 5. Variation of (*a*) $\phi(T)$, (*b*) α_0 and intensity $I_A(T)$ for the A rays during heating cycles, and (*c*) $\delta(\Delta n_b)(T)$ during heating (○) and cooling (○) cycles against temperature.

reproducible, even for relatively high-temperature rates (up to 0.25 K min^{-1}) which demonstrates the good quality of the thermal measurements and the absence of a thermal hysteresis, with 0.1 K uncertainty. All of the results presented above are discussed in the next section.

4. Discussion

Let us first study the variation of the deflected angles (α and β) on the incidence angle α_i quantitatively. To determine the path of beam across the crystal, three steps must be considered: the refractions on the incident sample face, the reflections and refractions on the domain walls and the refractions on the exit sample face. It is necessary to compute the optical slowness surfaces or index surfaces of light by solving the eigenvalues of the general wave equation, starting from Maxwell's curl equations. The resulting surface consists of two sheets since there are two allowed indices from each direction of propagation. Figure 6 shows these surfaces with as the coordinate axes x, y and z, the principal axes for the susceptibility χ and the orthorhombic axes a, b and c, respectively. In these coordinates χ is diagonal, with three different diagonal elements. The surfaces drawn in figures 6(b) and 6(c) correspond, for APFA, to the following values of the optical indices: $n_a = 1.5266$, $n_b = 1.4703$, $n_c = 1.5178$ (Andriyevski *et al* 1995). However, the propagation direction in the incident

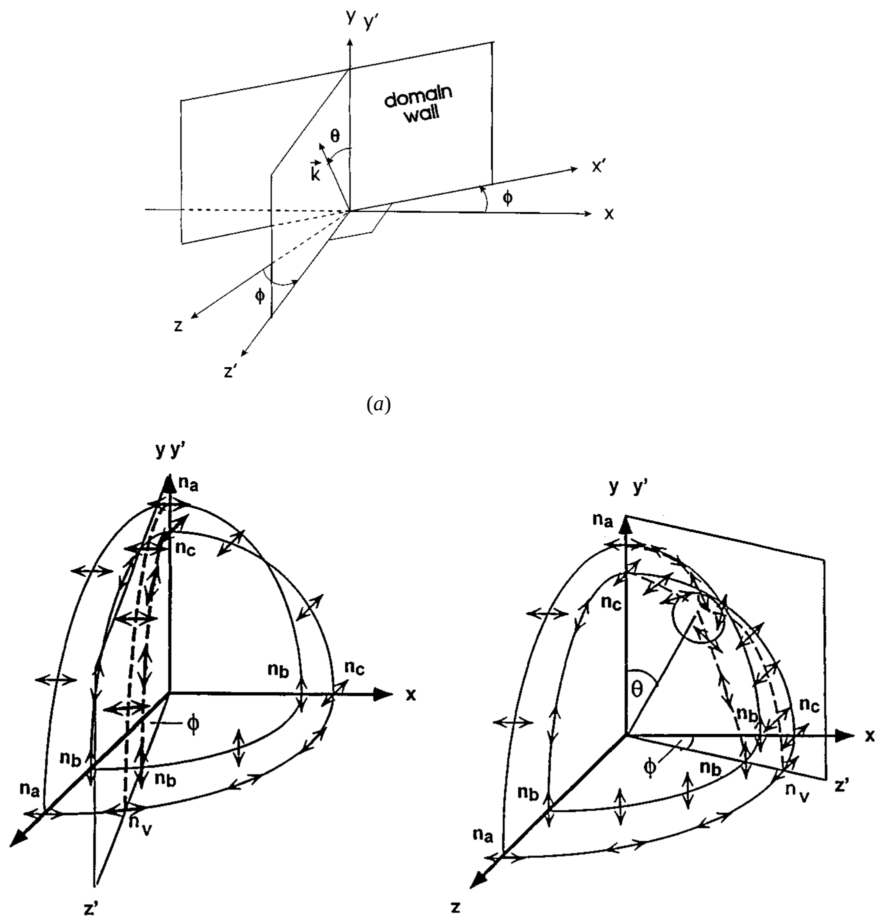

(*a*)

(*b*) (*c*)

Figure 6. (*a*) Principal axes for the susceptibility χ : x, y, z; domain walls and incident plane $y'z'$. (*b*) and (*c*) Index surfaces in APFA with incident plane corresponding to APFA1 walls and APFA2 walls, respectively.

plane is perpendicular to the domain walls' direction as illustrated by figure 6(*a*): these planes, which correspond to the orthorhombic planes, make the angle ϕ with the optical planes.

The properties of optical wave propagation are described by the section of the slowness surface in the incidence plane. The easiest way is to rotate the coordinate system of the susceptibility tensor by ϕ around the y-axis and then set $k_{x'} = 0$, i.e. the k vector is always inside the incidence plane. The propagation equation becomes

$$\begin{bmatrix} \left(\dfrac{\omega}{c_0}\right)^2 (1+\chi'_{11}) - k_{y'}^2 - k_{z'}^2 & 0 & \left(\dfrac{\omega}{c_0}\right)^2 \chi'_{13} \\ 0 & \left(\dfrac{\omega}{c_0}\right)^2 n_2^2 - k_{z'}^2 & k_{y'}k_{z'} \\ \left(\dfrac{\omega}{c_0}\right)^2 \chi'_{13} & k_{y'}k_{z'} & \left(\dfrac{\omega}{c_0}\right)^2 (1+\chi'_{33} - k_{y'}^2) \end{bmatrix} \begin{bmatrix} E_{x'} \\ E_{y'} \\ E_{z'} \end{bmatrix} = 0 \qquad (1)$$

with

$$\begin{aligned} 1+\chi'_{11} &= n_1^2 \cos^2\phi + n_3^2 \sin^2\phi \\ 1+\chi'_{33} &= n_1^2 \sin^2\phi + n_3^2 \cos^2\phi \\ \chi'_{13} &= \frac{\sin^2\phi}{2}(n_1^2 - n_2^2). \end{aligned} \qquad (2)$$

The desired section of the slowness surface is described by a bi-quadratic equation for k/ω. It consists of two branches, described by the two following solutions k_1/ω and $k_2\omega$ as shown by Meeks and Auld (1988):

$$\begin{aligned} \left(\frac{k}{\omega}\right)^2_{1,2} = & \left(\frac{n_2^2(1+\chi'_{33}) + \sin^2\theta[(1+\chi_{11})(1+\chi_{33}) - \chi'^2_{13}] + (1+\chi'_{11})n_2^2\cos^2\theta}{2c_0^2(n_2^2\cos^2\theta + (1+\chi'_{33})\sin^2\theta)}\right) \\ & \pm \frac{1}{2c_0^2(n_2^2\cos^2\theta + (1+\chi'_{33})\sin^2\theta)} \\ & \times \{[\sin^2\theta(\chi'_{13})^2 - (1+\chi'_{33}) - (1+\chi'_{11})n_2^2\cos^2\theta - n_2^2(1+\chi'_{33})] \\ & - 4[n_2^2\cos^2\theta + (1+\chi'_{33})\sin^2\theta][(1+\chi'_{11})(1+\chi'_{33})n_2^2 - n_2^2\chi'^2_{13}]\}^{1/2} \end{aligned} \qquad (3)$$

where θ is the angle between the $\vec{k}$ vector and the domain wall as shown in figure 6(*a*) and the indices 1, 2 and 3 correspond to x, y and z as usual.

The relations (2) and (3) allow us to calculate the solution k/ω as a function of θ, the angle between $\vec{k}$ and the y-axis. Slowness section curves in the $z'y'$ plane illustrate these solutions, as in figure 7(*a*) for the domain A and the domain B. Let us note that slowness curves for the opposite domain state are obtained by rotating the susceptibility tensor by π round the $b(y)$ crystal axis. The results of this rotation is to change z' into $-z'$ and y' into $-y'$. This result changes the sign of χ'_{13}. However, there is no change in the slowness section curves since χ'_{13} appears only as a squared term in relation (3). Hence, the slowness section curves are mirror symmetric about the $x'y'$ plane (the domain wall) as shown in figure 7(*a*). In general, the curves representing mode 1 (the slow wave) and mode 2 (the fast wave) are complicated ovaloides. The implications of this mirror symmetry are interesting in the prediction of the refracted and the reflected wave on the domain wall using the conservation of the k projection in the boundary (the domain wall) (Yariv and Yeh 1988). For example, figure 7(*a*) shows that an incident wave of the outer mode polarization (mode 1) $k_i^{(1)}/\omega$ will phase match into four waves, two refracted $k_t^{(1)}/\omega$ and $k_t^{(2)}/\omega$ and two reflected $k_r^{(1)}/\omega$ and $k_r^{(2)}/\omega$.

The incident wave of the inner mode (mode 2) $k_i^{(2)}/\omega$ will also phase match into four waves $k_t'^{(1)}/\omega$, $k_t'^2/\omega$, $k_r'^{(1)}/\omega$, $k_r'^{(2)}/\omega$. If the two incident polarizations are contained in the same beam

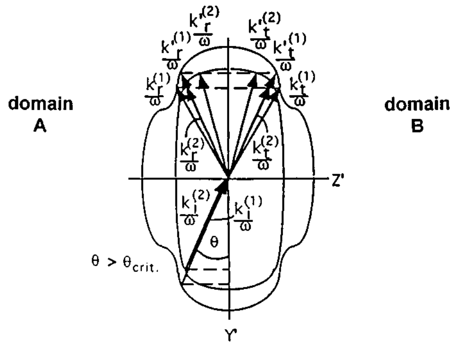

(*a*)

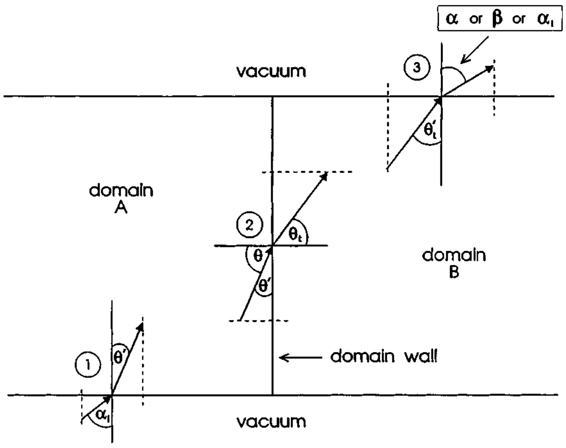

(*b*)

Figure 7. (*a*) Optical slowness curves for a $x'y'$ domain wall showing mirror symmetry and (*b*) the three steps for the wave propagation: refractions on the incident sample face and the exit sample face, refractions and reflections on a domain wall.

then two of the transmitted and two of the reflected waves will very nearly coincide. The result is that one sees a total of six waves (as in figure 1(*b*)) instead of eight. Similar slowness section curves can be drawn at the sample boundaries as shown in figure 7(*b*). Finally, it is possible to obtain relations as follows:

$$\begin{aligned}\frac{\omega}{c_0}\sin\alpha_i &= k_i^{(1)}(\theta_1')\sin\theta_1' = k_i^{(1)}\cos\theta_1\\ &= k_i^{(2)}(\theta_2')\sin\theta_2' = k_2^{(2)}\cos\theta_2\end{aligned} \tag{4}$$

$$\begin{aligned}k_i^{(1)}\sin\theta_1 &= k_t'^{(2)}\sin(\theta_{t_2})\\ k_i^{(2)}\sin\theta_1 &= k_t'^{(1)}\sin(\theta_{t_1})\end{aligned} \tag{5}$$

$$\begin{aligned}\frac{\omega}{c_0}\sin\alpha &= k_t^{(1)}\cos(\theta_{t_1})\\ \frac{\omega}{c_0}\sin\beta &= k_t^{(2)}\cos(\theta_{t_2})\end{aligned} \tag{6}$$

and to also calculate $\alpha(\alpha_i)$ and $\beta(\beta_i)$ using equations (1)–(3). The calculated variations are plotted in figures 3 and 4(*a*) (full curves) and appear in good agreement with the experimental

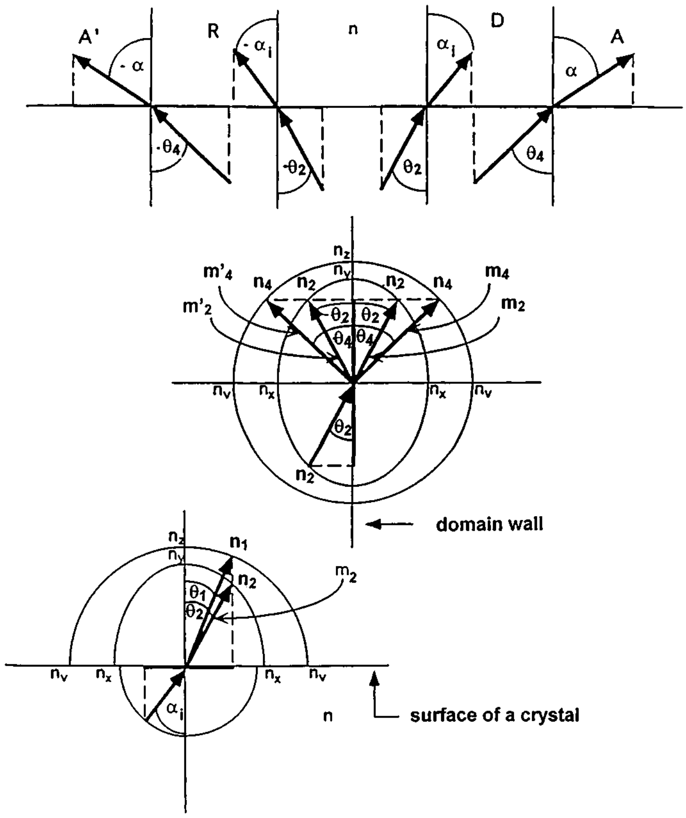

Figure 8. Constructions of the $\vec{k}$ wave vectors which correspond to the mode (m_2) of the wave after the refraction across the incidence face of the sample. The $\vec{k}$ vectors corresponding to rays A, A′,D and D′ at the exit face are indicated.

data. These numerical calculations give good results, but it is interesting to obtain even approximated analytical relations, allowing one to show the optical parameters' ageing on the α and β variations more clearly. Let us suppose, for example, that the intersections between the index surfaces and the incident plane are ellipses in a primary approximation and consider the $\vec{k}$ vectors in the three steps illustrated in figure 8. In this figure, the $\vec{k}$ vectors are parallel to the light rays only in the vacuum, out of the crystal. This is not the case inside the sample.

The primary incident light beam impinges on the sample face with incident angle α_i. The wave crosses this face and divides into two extraordinary waves, two different modes m_1 and m_2 corresponding to optical indices n_1 and n_2, and to angles θ'_1 and θ'_2 for the k vectors, respectively. For the mode m_2, it is possible to write the relation:

$$n_2 \sin\theta'_2 = n_0 \sin\alpha_i \tag{7}$$

where n_0 is the vacuum optical indice.

Then the wave (m_2) impinges a domain wall and is resolved into four secondary waves, namely m_2 and m_4 for the refracted waves and m'_2, m'_4 for the reflected waves. Due to the conservation of the tangent part of the wave vector and to the same shape of the index surfaces in both domains, the wave (m_2) crosses the domain wall without modification in the θ'_2 angle. In contrast, the orientation of the wave vector corresponding to the mode m_4 is given by

$$n_4 \cos\theta'_4 = n_2 \cos\theta'_2 \tag{8}$$

and this wave (m_4) corresponds, after refraction across the exit face of the sample, to

$$n_4 \sin\theta_4' = n_0 \sin\alpha. \tag{9}$$

From simple geometrical examinations using the equations of the ellipses shown in figures 6(*b*) and 6(*c*) it is possible to write n_2 and n_4 as follows:

$$n_2^2 = n_c^2 + \left(1 - \frac{n_c^2}{n_b^2}\right)\sin^2\alpha_i \tag{10}$$

$$n_4^2 = n_c^2 + n_v^2 - \frac{n_v^2 n_c^2}{n_a^2} + \left(\frac{n_v^2 n_c^2}{n_b^2 n_a^2} - \frac{n_c^2}{n_b^2}\right)\sin^2\alpha_i \tag{11}$$

with

$$n_v = n_a n_c \left[\frac{1 + \mathrm{tg}^2\phi}{n_c^2 + n_a^2 \mathrm{tg}^2\phi}\right]^{1/2}. \tag{12}$$

Using relations (7)–(12), it is possible to obtain the variation of α against α_i in the presented case corresponding to APFA1 wall:

$$\alpha = \pm \arcsin\left[\frac{1 + \mathrm{tg}^2\phi}{(n_a^2/n_c^2)\mathrm{tg}^2\phi + 1}\left(n_a^2 - n_c^2 + \frac{n_c^2}{n_b^2}\sin^2\alpha_i\right)\right]^{1/2}. \tag{13}$$

This equation possesses two real solutions for each α_i value, which correspond to the A and A′ rays' orientations. Using values previously given for n_a, n_b and n_c (Andriyevski *et al* 1995), it is possible to draw the curve $\alpha(\alpha_i)$ for the APFA1 wall as shown in figure 3. In the same way as the previous calculation performed for wave m_2, one proceeds in the case of wave (m_1) and obtains, for the APFA1 wall,

$$\beta = \pm \arcsin \frac{n_b}{n_c}\left[\frac{(n_a^2/n_c^2)\mathrm{tg}^2\phi + 1}{1 + \mathrm{tg}^2\phi}\sin^2\alpha_i + n_c^2 - n_a^2\right]. \tag{14}$$

The curve $\beta(\alpha_i)$ corresponding to the relation (14) is also drawn in figure 3 (broken curve). Figure 9 gives the difference between the experimental values and the theoretical values for $\alpha(\alpha_i)$ and $\beta(\alpha_i)$ as well as the difference between the approximated model and the general case. It is possible to note that the accuracy of the experimental data is not very good (with an uncertainty between 0.1° and 0.5°) when the deflected beam is close to the undeflected beam D, i.e. for small α_i values. The uncertainty is, obviously, also important when the $\alpha(\alpha_i)$ and $\beta(\beta_i)$ curves present horizontal or vertical tangents. In contrast the approximated model gives very good results for $\alpha(\alpha_i)$, except in the vertical tangent region. The differences are comparable to the experimental uncertainty for β variation in all of the α_i range.

The same approximated calculations can be performed in the APFA2 wall situation and the following relations are obtained:

$$\alpha = \pm \arcsin \frac{n_b}{n_a}\left[\frac{(n_a^2/n_c^2)\mathrm{tg}^2\phi + 1}{1 + \mathrm{tg}^2\phi}\sin^2\alpha_i + n_a^2 - n_c^2\right]^{1/2} \tag{15}$$

$$\beta = \pm \arcsin\left[\frac{1 + \mathrm{tg}^2\phi}{(n_a^2/n_c^2)\mathrm{tg}^2\phi + 1}(n_c^2 - n_a^2\sin^2\alpha_i)\right]^{1/2}. \tag{16}$$

These approximated relations correspond to the broken curves in figure 4(*a*), whereas the full curves correspond to the general calculation. The quality of the approximation can be easily appreciated. The curves drawn with relations (15) and (16) cross each other at the value $\alpha_i = 35.86°$, but it is only the result of the model. It is not possible to measure real deflected beam intensities near this value of α_i due to the proximity of the deflected beams A and B and the D beam and, also, to their small relative intensities. However, figure 6(*c*) allows one to understand

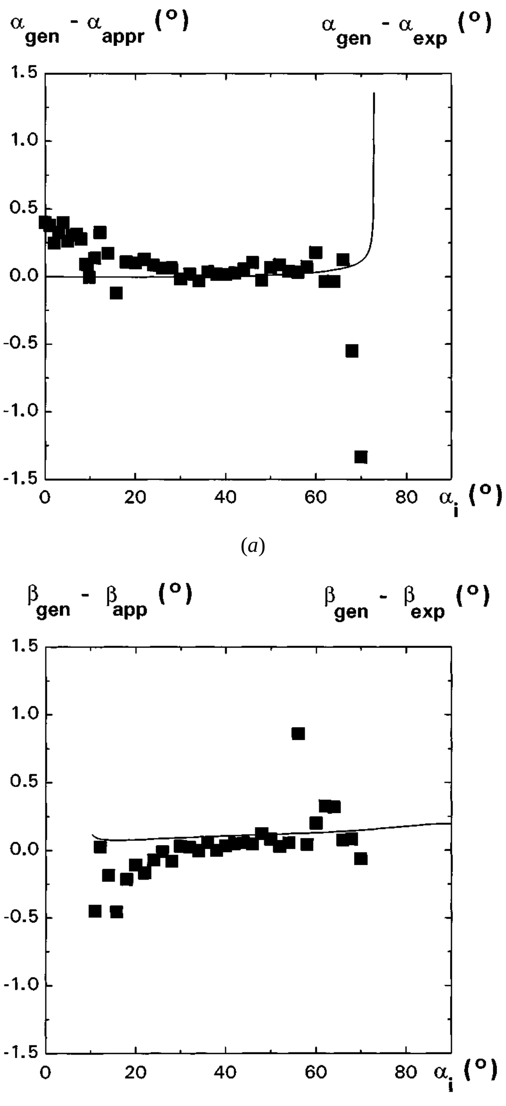

Figure 9. The difference between the deflected angles calculated by the general model and the experimental data (■), and the approximated model (full curve): (*a*) = $\Delta\alpha(\alpha_i)$, (*b*) $\Delta\beta(\alpha_i)$.

the results obtained in figures 4(*a*) and 4(*b*): for the APFA2 walls in the defined experimental conditions the incidence plane $y'z'$, which is perpendicular to the domain walls, is close to the optical principal plane containing the optical axis. The two sheets of the index surface cross each other only in the optical axis plane. Then the A and B beams do not really cross around $\alpha_i = 35°$. In contrast the polarization of the light in these regions rotates, as illustrated on figures 4(*b*) and 6, when θ changes i.e. when α_i changes. Obviously, it is possible to predict this rotation of the light polarization using relation (1) for each orientation θ of the $\vec{k}$ vectors. These results demonstrate the interest of the deflected beam measurements ($\alpha(\alpha_i)$, $\beta(\alpha_i)$ and light polarization) to easily obtain information on the optical properties of the crystal which is twinned.

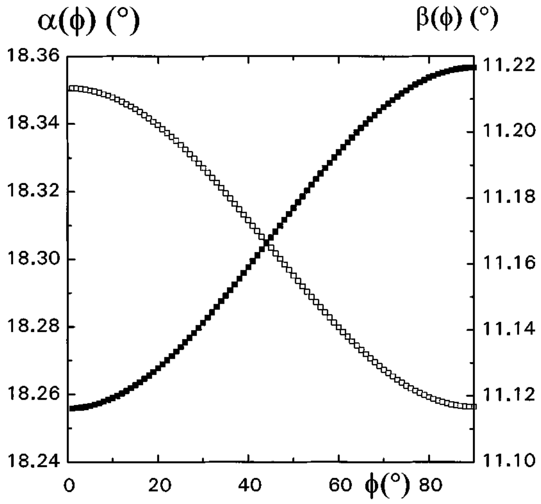

Figure 10. Variation of the deflected angles α (□) and β (■) against the tilt angle ϕ in the case of APFA1 walls with $\alpha_i = 15^{\circ}$.

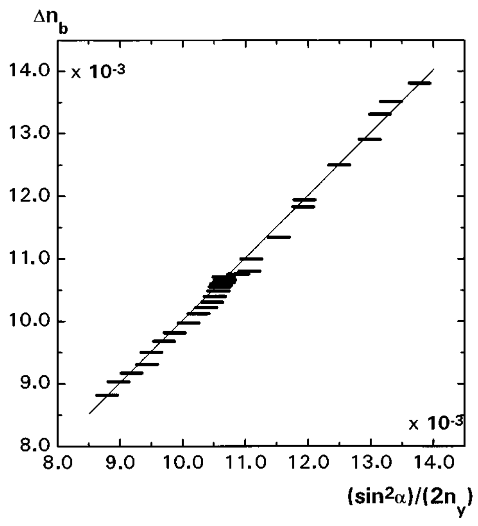

Figure 11. Variation of the birefringence Δn_b for the light propagating along the b axis against $\sin^2 \alpha_0/2n_c$ for the APFA1 walls.

Taking into account the quality of the approximated model as demonstrated previously, it is possible to use relations, such as (13)–(16), to study the effects of the optical properties of the crystal on the deflected angles. For example, the influence of the ϕ angle on the α and β angles is illustrated in figure 10 for the APFA1 walls: a variation of ϕ between 0° and 90° induces only a modification in α and β values of the order of, in general, about 1%. Then, it is interesting to correlate the deflected angle with the optical indices. A very simple experimental case is given by the measurement of the angle α with $\alpha_i = 0$. Using relation(13) it is easy to write:

$$\sin^2\alpha_0 = 2n_c\Delta n_b + \Delta n_b^2\frac{1-3\mathrm{tg}^3\phi}{1+\mathrm{tg}^2\phi} + 4\frac{\Delta n_b^3}{n_y}\frac{\mathrm{tg}^2\phi(\mathrm{tg}^2\phi-1)}{(1+\mathrm{tg}^2\phi)^2} + \varepsilon \tag{17}$$

or if the birefringence $\Delta n_b = n_a - n_c$ for the light propagating along the b-axis is small

$$\sin^2\alpha_0 = 2nc\Delta n_b + \varepsilon' \tag{18}$$

with the ε and ε' functions of n_y, ϕ and Δn_b^p (the exponent p is at least four in (17) and two in (18)). Relation (18) is well illustrated by figure 11, which shows the quasi-linear dependence between $\sin^2\alpha_0$ and the birefringence Δn_b. This result is very conclusive because the intensities of the deflected beams in APFA are relatively small (a few per cent of the incident beam, or less) and the divergence of these beams change with temperature.

5. Conclusion

The deflected beams, A and B, have been studied in APFA against the angle of the incident beam α_i, especially from the point of view of the deflected angle and light polarization. This study presents two different situations. In the first (the APFA1 case) the incidence plane is far away from the optical principal plane containing the optical axis: A and B beams are always clearly separated as α_i varies and their polarizations are almost perpendicular, without noticeable variation. In contrast in the APFA2 case, the incidence plane is close to the optical axis. For $\alpha_i = 35$–36°, the A and B beams are close to each other and their polarizations, which are always approximately perpendicular, are exchanged. That proves the vicinity to the optical axis as illustrated in figures 3, 4 and 6. Then it is possible in the situation described in figure 1(a), to easily obtain information on a biaxial crystal as shown in figure 6. A general model allows us to numerically calculate the orientations of the $\vec{k}$ wave vectors and the light polarizations which correspond to the deflected beams. It is also possible to obtain analytical relations $\alpha(\alpha_i, \phi, n_i)$ and $\beta(\alpha_i, \phi, n_i)$ assuming that the intersections between the index surfaces and the incident plane are ellipses. This approximated model gives results that are in good agreement with the experimental data and with the results calculated in general case if the birefringence is not greater than 10^{-2}. The relations, such as (13)–(16), can be written in all crystals and the following paper (Staniorowski and Bornarel 2000), concerning GMO crystals, demonstrates the better accuracy of this numerical approach compared to the Huygens construction. An important result is analytically and experimentally demonstrated on the variation of α and β as a function of the optical properties of the crystal: the tilt angle ϕ does not play a significant role and $\sin^2\alpha_0$ is, with a good accuracy, proportional to the birefringence for a light propagating in the crystal axis parallel to the normal incident beam ($\alpha_i = 0^\circ$). Thus, it is interesting to study the transitions and the domains in ferroelastic crystals: the birefringence is easily measured by classical methods when the sample exhibits only a few domains. However, this measurement becomes difficult for dense domain textures. The deflection can supply the classical techniques in the situation of twinned crystals. This can also be useful in such applications as electromodulators. APFA is not a good case for such applications because the deflected beams have small intensities. Other crystals seem more promising (Salvestrini *et al* 1997, Guilbert *et al* 1998). In all cases, the intensities of the deflected beams must be now studied: not only the effect of the optical properties of the crystal and of the light polarization and the wave length, but also the relative importance of the deflection phenomenon and diffraction phenomena.

Acknowledgment

This work was partly supported by the University of Wroclaw under grant 2016/IFD/98 and the French Government.

References

Andriyevski B, Czapla Z and Stadnyk V 1995 *Acta Phys. Pol.* **87** 611
Avkhutskii L M, Davidovich R L, Zemnukhova L A, Gordienko P, Urbonaviaus V and Grigas J 1983 *Phys. Status Solidi* b **116** 483
Bornarel J, Staniorowski P and Czapla Z 1997 *Phys. Status Solidi* **203** 59
Czapla Z and Dacko S 1994 *Ferroelectrics* **146** K1
Guilbert L, Salvestrini J P, Kolata P, Abrial F X, Fontana M D and Czapla Z 1998 *J. Opt. Am.* B **15** 1009
Hatano J, Iwauchi K, Sato M, Tsukamoto T, Saïto S and Murashiro K 1993 *Ferroelectrics* **149** 15
Hill R M and Ichiki S K 1964 *Phys. Rev.* A **135** 1640
Hill R M, Herman G F and Ichiki S K 1965 *J. Appl. Phys.* **36** 3672
Kinoshita S, Kutsuzawa S, Shimada Y and Yagi T 1994 *Phys. Rev.* B **50** 5834
Koralewski M and Szafranski M 1988 *Ferroelectrics* **80** 269
——1989 *Ferroelectrics* **97** 233
Legrand Y, Rouéde D, Wienold J and Glinnemann J 1998 *J. Phys. Soc. Japan* **67** 1451
Meeks S W and Auld B A 1988 *Adv. Electron. Electron. Phys.* **71** 251
Mukhopadhyay R, Goyal P S and Carlile C J 1993 *Phys. Rev.* B **48** 2880
Mukhopadhyay R, Goyal P S and Rao K R 1991 *Phys. Status Solidi* **165** 335
Nakamura N 1986 *Z. Naturf.* a **41** 243
Salvestrini J P, Guilbert L, Fontana M D and Czapla Z 1997 *J. Opt. Soc. Am.* B **14** 2818
Staniorowski P and Bornarel J 2000 *J. Phys.: Condens. Matter* **12** 669
Szafranski M 1992 *Ferroelectrics* **129** 55
Tsukamoto T 1984 *Japan. J. Appl. Phys.* **23** 424
Tsukamoto T and Futama H 1993 *Phase Transitions* **45** 59
Tsukamoto T, Hatano J and Futama H 1982 *J. Phys. Soc. Japan* **51** 3948
——1984 *J. Phys. Soc. Japan* **53** 838
Tsukamoto T, Komukae M, Suzuki S, Futama H and Makita Y 1983 *J. Phys. Soc. Japan* **52** 3966
Tsukamoto T, Sato T, Hatano J and Futama H 1985 *Japan. J. Appl. Phys.* **24** 559
Udovenko A A *et al* 1987 *Koord. Khim* **13** 558
Vehara H, Ogawa S, Tatemori S, Hatano J, Saïto S, Saïto H and Okabe E 1996 *Japan. J. Appl. Phys.* **35** 5054
Waskowska A and Czapla Z 1989 *Crystal Res. Technol.* **24** 1259
Yariv A and Yeh P 1988 *Optical Waves in Crystals* (New York: Wiley)